

# Deep Learning Forecasting of the U.S. Aggregate Bond Index

Ajay Kumar Verma<sup>1</sup>, Jul Jon Ramirez General<sup>2</sup>, Yvan Landry Ndzonde Fonkou<sup>3</sup>

May 2026

## Abstract

This study looks at the statistical properties and predictability using deep learning methods of the U.S. aggregate bond index in daily observations spanning 2018 to February 2026. We first establish that index *levels* are extremely persistent and consistent with unit-root behavior (Dickey and Fuller), while *log returns* are covariance-stationary with weak linear dependence and pronounced volatility clustering characteristic of ARCH-type processes (Engle; Bollerslev). Motivated by the trade-off between stationarity and information retention, we construct a “stationary but maximally persistent” representation via fractional differencing (Granger and Joyeux; Hosking) following the procedure of López de Prado, and evaluate short-horizon forecast using two neural paradigms: (i) Multilayer Perceptrons (MLPs) trained on lagged vectors with joint lag-length and hyperparameter tuning (Hornik et al.; Rumelhart et al.); and (ii) Convolutional Neural Networks (CNNs) trained on Gramian Angular Field (GAF) image encodings (Wang and Oates). Empirically, MLPs match the strong naive persistence benchmark on levels, collapse toward near-zero forecasts on returns, and achieve the strongest incremental performance on the fractionally differenced series, where moderate dependence remains but unit-root drift is attenuated. In contrast, CNN–GAF models deliver consistently negative out-of-sample  $R^2$  across all three representations. Overall, the results imply that, for short-horizon forecasting of broad bond indices, the primary determinant of predictive performance is the transformation of the series-its degree of stationarity and memory-rather than architectural complexity. Lag-based models remain competitive under persistence, while GAF-based CNNs are better suited to pattern-based tasks than to persistence-dominated next-step prediction.

**Keywords:** bond index forecasting; fractional differencing; multilayer perceptron; Gramian Angular Field; convolutional neural network; unit root; long memory.

---

<sup>1</sup>Independent Researcher (azay.verma@gmail.com) , <sup>2</sup>Bangko Sentral ng Pilipinas (generaljr@bsp.gov.ph) , <sup>3</sup>Independent Researcher (yvanndzonde@gmail.com)

## 1. Introduction and Objectives

The predictability of financial time series at short horizons has been researched by financial economists and practitioners for decades (Fama; Campbell and Shiller). The development of deep learning methods have renewed this inquiry, offering flexible function approximators capable of extracting nonlinear structure from high-dimensional inputs (LeCun et al., “Deep Learning”). But, the application of such methods to financial forecasting considering the statistical properties of index prices—non-stationarity, volatility clustering, fat tails, etc - impose specific requirements on data preprocessing, model design, and evaluation that differ substantially from those encountered in image recognition or natural language processing (Hamilton).

The present study investigates the statistical properties and the short-horizon predictability of the U.S. Aggregate Bond Index. Using 2,000 daily observations spanning 2018–2026, we pursue seven interconnected objectives: First, to characterize the distributional behavior of index levels, including measures of dispersion, skewness, and kurtosis. Second, we formally assess unit-root behavior in levels leveraging the Augmented Dickey–Fuller (ADF) test (Said and Dickey), confirming whether the index is integrated of order one,  $I(1)$ . Third, we establish that log returns are approximately  $I(0)$  by documenting weak autocorrelation, rapid mean reversion, and heteroskedastic variance dynamics. Fourth, we implement the fractional differencing procedure of López de Prado to construct a near-stationary representation that preserves long-memory structure, selecting the differencing order via an ADF  $p$ -value diagnostic. Fifth, we tune the lag length and hyperparameters of a feed-forward MLP and test whether nonlinear lag-based models improve one-step-ahead forecasts beyond naive persistence benchmarks across levels, log returns and the fractionally differenced series. Sixth, we transform each series into Gramian Angular Field images and check whether CNNs can extract predictive patterns from this image representation. Finally, we compare the two architectures in terms of inductive bias, representation choice, and the statistical properties of the underlying time series, providing a theoretically grounded account of the observed performance differences.

The study contributes to a growing literature on machine learning methods in finance (López de Prado; Gu et al.) by demonstrating that the selection of data representation and not the model complexity is often the binding constraint on predictive performance for highly persistent financial series.

## 2. Empirical Analysis of U.S. Aggregate Bond Index Levels

### 2.1 Sample and Distributional Properties

The sample spans from March 8, 2018 to February 20, 2026, comprising  $n = 2,000$  daily observations of index levels. Figure 1 shows the full time series of the U.S. Agg Bond Index over this period.

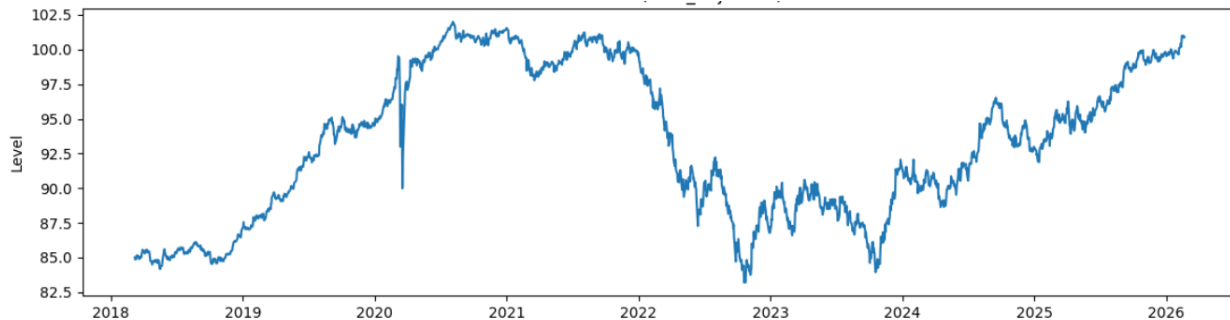


Figure 1: Daily closing levels of the U.S. Agg Bond Index, March 2018–February 2026.

Summary statistics for the index level are shown in Table 1. The unconditional distribution of the Index level appears approximately symmetric: the estimated skewness of  $-0.034$  is economically negligible, and the excess kurtosis of  $-1.298$  denotes a platykurtic distribution relative to the Gaussian benchmark, with lighter tails but a flatter peak. Such behavior is consistent with index levels observed over a bounded sample horizon, where extreme realizations are naturally constrained by the mean-reversion of long-horizon bond yields. Over the period, the index fluctuates between 83.19 and 101.99, with a standard deviation of 5.34. The interquartile interval spanning the 5th to 95th percentiles (approximately 85.0 to 100.9) confirms moderate unconditional dispersion. The maximum drawdown of  $-18.43\%$  represents the largest peak-to-trough reduction during the period and is consistent with the bond market changes associated with the 2022–2023 interest-rate normalization cycle (Hamilton).

Although the unconditional distribution appears stable in scale and symmetry, price levels of broad fixed-income indices are typically highly persistent and exhibit unit-root behavior (Nelson and Plosser). The relatively narrow dispersion and bounded range therefore do not imply stationarity; formal statistical testing is required. In financial economics, the standard paradigm distinguishes between non-stationary levels ( $I(1)$ ) and stationary first differences or log returns ( $I(0)$ ), so that econometric inference is appropriately conducted on returns rather than on raw price levels (Engle and Granger).

### 2.2 Autocorrelation Structure and Implications for Stationarity

The autocorrelations of daily index levels are shown in Table 2. The lag-1 auto-correlation is exceptionally high ( $\rho_1 = 0.998$ ), indicating near-perfect persistence between consecutive trading

Table 1: Summary statistics for U.S. Aggregate Bond Index levels ( $n = 2,000$ ).

Statistic	Value
Mean	93.260
Standard Deviation	5.335
Minimum	83.191
1st Percentile	84.372
5th Percentile	84.994
Median	93.600
95th Percentile	100.929
99th Percentile	101.398
Maximum	101.991
Skewness	-0.034
Excess Kurtosis	-1.298
Maximum Drawdown	-18.43%

days. Even at a monthly horizon of 21 trading days, the autocorrelation remains strong ( $\rho_{21} = 0.963$ ), and at the quarterly frequency ( $\rho_{63} = 0.874$ ) it remains substantial. Only at the annual horizon does persistence reduce more noticeably ( $\rho_{252} = 0.265$ ), yet it remains clearly positive.

Table 2: Sample autocorrelations of U.S. Aggregate Bond Index levels at selected lags.

Lag	Autocorrelation
1 day	0.998
5 days	0.991
21 days (1 month)	0.963
63 days (1 quarter)	0.874
252 days (1 year)	0.265

This slowly decaying autocorrelation function is a hallmark of integrated processes (Box et al.). For a covariance-stationary process, autocorrelations generally decline toward zero at a geometric rate, whereas unit-root processes exhibit very high autocorrelations at short lags and only gradual mean reversion. The observed pattern is consistent with the behavior of an  $I(1)$  process of below form

$$P_t = P_{t-1} + \varepsilon_t, \tag{1}$$

where  $\varepsilon_t$  is a mean-zero innovation. This provides preliminary evidence against stationarity in levels, which motivates formal unit-root testing and the subsequent analysis of log returns and fractionally differenced transformations.

### 2.3 Unit-Root Testing using the Augmented Dickey–Fuller Test

To formally evaluate the stationarity of the index level, we use the Augmented Dickey–Fuller (ADF) test (Dickey and Fuller; Said and Dickey) under two specifications: a) a model with a constant only, and b) a model with both a constant plus a deterministic time trend. The ADF test evaluates the null hypothesis ( $H_0$ ) that the series contains a unit root.

Table 3: ADF test for U.S. Aggregate Bond Index levels (constant only).

Statistic	Value
ADF Statistic	−1.3715
$p$ -value	0.5959
Lags Used	7
Observations	1,992
Critical Value (1%)	−3.4336
Critical Value (5%)	−2.8630
Critical Value (10%)	−2.5675
AIC	1,328.415

Table 4: ADF test for U.S. Aggregate Bond Index levels (constant and trend).

Statistic	Value
ADF Statistic	−1.3798
$p$ -value	0.8667
Lags Used	7
Observations	1,992
Critical Value (1%)	−3.9633
Critical Value (5%)	−3.4127
Critical Value (10%)	−3.1283
AIC	1,330.387

Under the constant-only specification, the test statistic of  $-1.3715$  is substantially above all critical values in absolute magnitude ( $-1.3715 > -2.8630$  at the 5% level), and the  $p$ -value of 0.596 is far above conventional significance thresholds, thus providing no evidence against the null hypothesis of having a unit root. Adding a deterministic time trend does not alter this conclusion: the test statistic of  $-1.3798$  remains above critical values, with the  $p$ -value rising to 0.867, yielding even weaker evidence against  $H_0$ . Taken together with the extremely high short-horizon autocorrelations and the slow decay of the empirical autocorrelation function documented above, both ADF specifications strongly support the characterizing the U.S. Aggregate Bond Index level series as an integrated process of order one,  $I(1)$ . Hence, statistical inference, volatility modeling, and predictive analysis should be conducted on first differences (log returns) rather than on raw levels.

### 3. Log Returns: Stationarity, Dependence, and Volatility Dynamics

#### 3.1 Visual Inspection and Mean Behavior

Figure 2 shows the daily log returns of the U.S. Aggregate Bond Index. Log returns correspond to first differencing in logarithms. If the level process is approximately  $I(1)$  as established in Section 2, the log-return series should be approximately  $I(0)$  stationary with finite mean and variance (Nelson and Plosser). The series hovers around zero with no visible deterministic trend, strongly supporting this characterization.

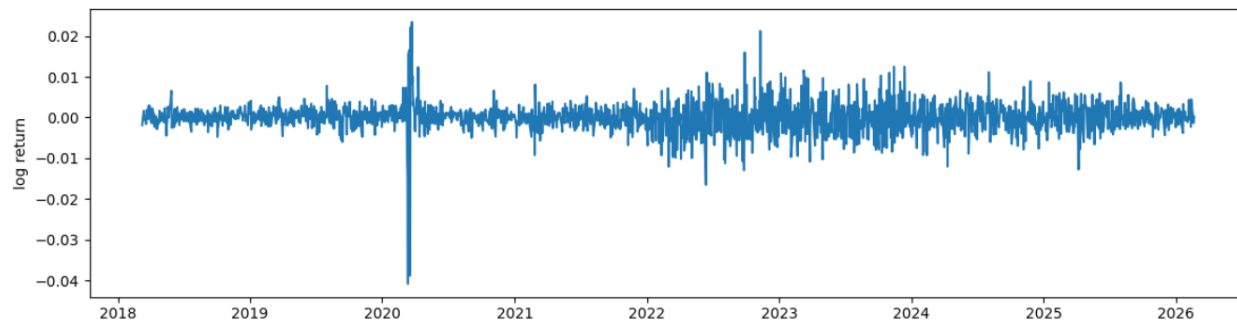


Figure 2: Daily log returns of the U.S. Aggregate Bond Index, 2018–2026.

A key feature visible in the figure is volatility clustering: distinct periods of low volatility (2018–2019) proceeds with a sharp spike in early 2020 associated with the COVID-19-related bond market shock, elevated and persistent volatility during 2022–2023 corresponding to the interest-rate normalization cycle, and gradual moderation thereafter. This pattern is a canonical stylized fact of financial time series (Cont), commonly modeled using ARCH and GARCH frameworks (Engle; Bollerslev), and suggests that conditional heteroskedasticity is a dominant feature of this series. The occasional large spikes in both directions imply heavy-tailed return distributions relative to the Gaussian benchmark and potential asymmetry during stress episodes, consistent with the broader literature on fat tails in financial returns (Mandelbrot).

#### 3.2 Formal Stationarity Tests and Autocorrelation Structure

Table 5 shows the results of the ADF test for the log-return series. The test statistic of  $-17.8123$  is below all critical values in absolute magnitude ( $-17.8123 < -3.4336$  at the 1% level), and the  $p$ -value is effectively zero, leading to decisive rejection of the unit-root null hypothesis. This provides overwhelming statistical evidence that the log-return series is covariance-stationary.

The autocorrelation structure of the log-return series, shown in Table 6, is in stark contrast to the level series. Autocorrelations are small in magnitude over all lags: the lag-1 autocorrelation is 0.027, and at the quarterly horizon (63 trading days) it remains modest at 0.064; at the annual horizon it is essentially zero. This rapid decay toward zero is characteristic of stationary return

Table 5: ADF test for U.S. Aggregate Bond Index log returns (constant specification).

Statistic	Value
ADF Statistic	-17.8123
<i>p</i> -value	< 0.001
Lags Used	6
Observations	1,992
Critical Value (1%)	-3.4336
Critical Value (5%)	-2.8630
Critical Value (10%)	-2.5675
AIC	-16,504.110

processes and aligns with the weak-form efficiency hypothesis (Fama), under which linear structure predictability in returns is limited. Formally, the evidence supports the representation

$$r_t = \mu + \varepsilon_t, \tag{2}$$

where  $\varepsilon_t$  is a mean-zero stationary disturbance exhibiting conditional heteroskedasticity. These findings establish that the U.S. Aggregate Bond Index is well-characterized as an  $I(1)$  process in levels and an  $I(0)$  process in returns, consistent with canonical asset pricing theory and the standard prescription for modeling and forecasting (Campbell and Shiller).

Table 6: Sample autocorrelations of U.S. Aggregate Bond Index log returns.

Lag	Autocorrelation
1 day	0.027
5 days	0.002
21 days (1 month)	0.019
63 days (1 quarter)	0.064
252 days (1 year)	-0.002

## 4. Fractional Differencing: Theory, Diagnostics, and Implementation

### 4.1 Classical Differencing and the Over-Differencing Problem

The empirical results of Sections 2 and 3 show that index levels are  $I(1)$  and that log returns are  $I(0)$ , which justify first differencing (in logarithms) as the canonical transformation for reducing the stochastic trend. An important concern in this context is whether first differencing is excessive, that is, whether the original series were already stationary and differencing merely introduces artificial negative autocorrelation and amplifies noise. The empirical autocorrelation structure of returns does not exhibit such behavior, and the ADF test for levels provides no evidence of prior stationarity; first differencing is therefore appropriate (Box et al.).

However, integer differencing can also be problematic in a different direction: by applying the operator  $(1 - L)^1$  to eliminate the stochastic trend, one may inadvertently discard low-frequency dependence that carries economically relevant predictive information. This observation motivates the more general framework of fractional differencing (Granger and Joyeux; Hosking), in which the differencing operator is parameterized continuously as  $(1 - L)^d$  for  $d \in (0, 1)$ . Using the binomial expansion,

$$(1 - L)^d = \sum_{k=0}^{\infty} w_k L^k, \quad w_k = (-1)^k \binom{d}{k} = (-1)^k \frac{d(d-1) \cdots (d-k+1)}{k!}, \quad (3)$$

the fractionally differenced series is

$$\tilde{P}_t = (1 - L)^d P_t = \sum_{k=0}^{\infty} w_k P_{t-k}. \quad (4)$$

The weights  $w_k$  decay hyperbolically at rate  $|w_k| \sim k^{-(1+d)}$  for large  $k$ , generating the long-memory dependence that distinguishes fractional differencing from integer differencing (where all weights beyond  $k = 1$  are exactly zero for  $d = 1$ ). Unlike exponential decay, this hyperbolic decay persists low-frequency structure in the transformed series. The practical significance for machine learning pipelines is threefold: many algorithms assume stationarity implicitly; excessive differencing can degrade the signal-to-noise ratio; and long-memory components may contain predictive features that would be destroyed by full integer differencing (Baillie; López de Prado).

## 4.2 The López de Prado “Stationary but Maximally Persistent” Criterion

López de Prado proposes selecting the minimum differencing order  $d^*$  such that the transformed series achieves stationarity, while retaining the maximum admissible long-memory structure:

$$d^* = \min\{d \mid (1 - L)^d P_t \text{ is stationary}\}. \quad (5)$$

Generally, we evaluate the fractional differencing transformation over a grid of  $d$  values, apply an ADF test to each transformed series, and select the smallest  $d$  for which the unit-root hypothesis is rejected at a chosen significance level. The philosophical distinction from classical econometrics is important: the standard approach removes integration fully by setting  $d = 1$ , while the fractional ML approach eliminates only the minimum integration required, preserving the maximum amount of memory for downstream modeling. This is particularly relevant in a machine learning context, where long-memory features may be informative predictors that would be lost under full differencing (Baillie; López de Prado).

Figure 3 illustrates this diagnostic for the U.S. Aggregate Bond Index. The left panel reports ADF  $p$ -values as a function of  $d \in [0, 1]$  for the original-scale level series, while the right panel shows the corresponding diagnostics for the log transformed series.

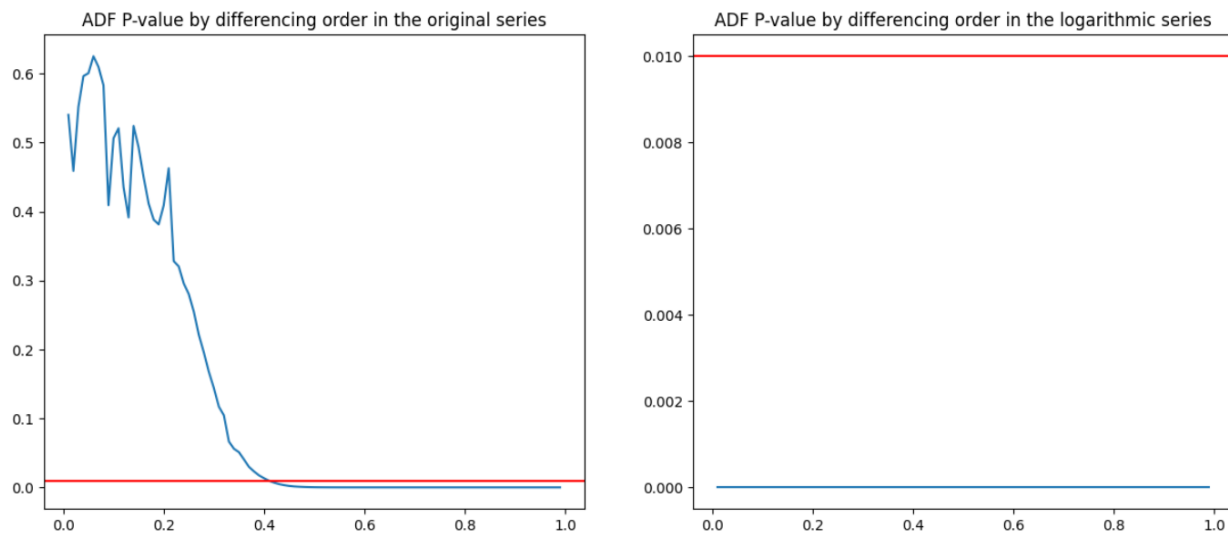


Figure 3: ADF  $p$ -value as a function of differencing order  $d$  for the original-scale level series (left) and the log-transformed series (right). The red horizontal line denotes the 1% significance threshold.

For the original levels, ADF  $p$ -values remain above conventional significance thresholds for small  $d$ , confirming the failure to reject the unit-root null hypothesis documented in Section 2. As  $d$  increases, the  $p$ -value declines monotonically, crossing the 1% threshold only at approximately  $d^* \approx 0.40$ – $0.45$ . This implies that a meaningful degree of differencing is required before the series achieves stationarity under the ADF tests, and that fractional differencing at  $d \approx 0.4$  provides a near-stationary representation while retaining substantially more memory than full integer differencing.

For the log-transformed series, the ADF  $p$ -value is effectively zero across the entire grid, confirming that log returns are unambiguously stationary for any positive differencing order.

### 4.3 The Fractionally Differenced Level Series at $d = 0.4$

Motivated by the diagnostic of Figure 3, we apply fractional differencing at  $d = 0.4$  to the U.S. Aggregate level series, arriving at the transformed process

$$\tilde{P}_t^{(0.4)} = (1 - L)^{0.4} P_t = \sum_{k=0}^K w_k P_{t-k}, \quad (6)$$

when the infinite expansion is truncated at a finite lag  $K$  using a weight-threshold criterion ( $|w_K| < 10^{-5}$ ). Because the operator requires  $K$  lagged observations, the effective sample spans from April 25, 2019 to February 20, 2026, with  $n = 1,716$  observations. The transformed series is shown in Figure 4.

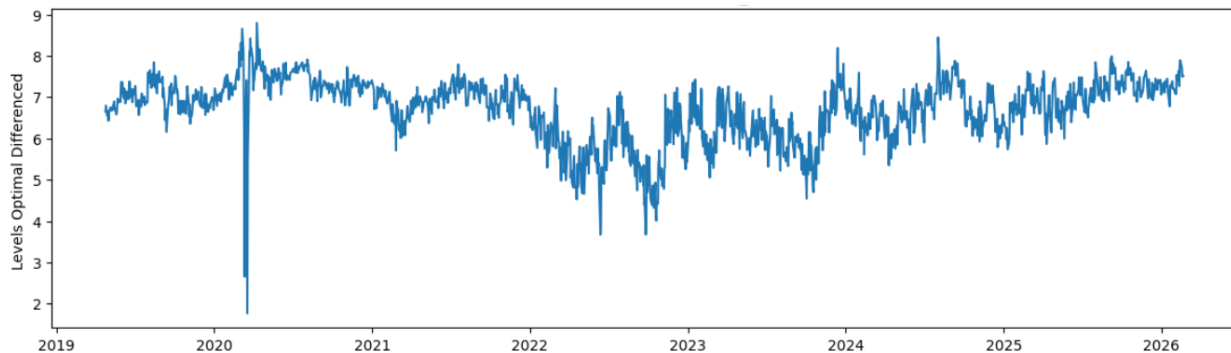


Figure 4: U.S. Aggregate Bond Index levels after fractional differencing at  $d = 0.4$  (“stationary but maximally persistent” representation).

Several features of the transformed series warrant discussion. The dominant stochastic trend present in the raw level series is materially attenuated: the series fluctuates around a relatively stable band, consistent with near-stationarity. At the same time, slow-moving multi-month swings persist in the transformed series, reflecting the deliberate preservation of low-frequency dependence relative to full first differencing (Hosking). A pronounced negative spike in early 2020 reflects the response of the fractional filter which applies a weighted sum of many past observations to the sharp COVID-19 shock in the underlying level series. Such spikes are informative about structural breaks and market dislocations but can also create influential outliers in model estimation, warranting robust scaling or outlier-aware loss functions. Elevated variability during 2022–2023 is consistent with the interest-rate regime shift and suggests that conditional heteroskedasticity persists even after fractional differencing.

Summary statistics and autocorrelations for the transformed series are presented in Tables 7 and 8, respectively. The distribution is asymmetric (skewness =  $-1.09$ ) and heavy-tailed (excess

kurtosis = 2.22), reflecting the influence of stress episodes that manifest as transitory shocks after applying the long-memory filter. The lag-1 autocorrelation reduces from near unity in levels to 0.860 after fractional differencing, with smooth decay across horizons precisely the intended intermediate profile between the near-random-walk behavior of levels and the near-white-noise behavior of returns. Formal ADF testing (Table 9) under the constant-only specification yields a  $p$ -value of 0.013, marginally rejecting the unit-root null at the 5% level; under the constant-plus-trend specification, the  $p$ -value rises to 0.062, reflecting borderline behavior consistent with the deliberate choice of a small  $d$  to preserve memory. This borderline stationarity is not a defect of the transformation; it reflects the intended trade-off between integration removal and memory preservation.

Table 7: Summary statistics for fractionally differenced levels ( $d = 0.4$ ,  $n = 1,716$ ).

Statistic	Value
Mean	6.716
Standard Deviation	0.743
Minimum	1.768
1st Percentile	4.558
5th Percentile	5.300
Median	6.869
95th Percentile	7.648
99th Percentile	7.951
Maximum	8.796
Skewness	-1.088
Excess Kurtosis	2.215

Table 8: Sample autocorrelations of fractionally differenced levels ( $d = 0.4$ ).

Lag	Autocorrelation
1 day	0.860
5 days	0.713
21 days (1 month)	0.565
63 days (1 quarter)	0.398
252 days (1 year)	0.189

Table 9: ADF tests for fractionally differenced levels ( $d = 0.4$ ).

Specification	ADF Stat.	$p$ -value	5% Critical	Decision (5%)
Constant ( $c$ )	-3.338	0.013	-2.863	Reject $H_0$
Constant + Trend ( $ct$ )	-3.327	0.062	-3.413	Fail to reject $H_0$

The  $d = 0.4$  transformation can be interpreted as a principled compromise between raw levels and log returns. Relative to levels ( $d = 0$ ), it is substantially closer to stationary and more suitable for machine learning algorithms that assume distributional stability over time (López de

Prado). Relative to log returns ( $d = 1$ ), it retains richer low-frequency dependence that may be exploited by predictive models if those dependencies are genuine rather than attributable to stochastic drift (Baillie). In practice, the utility of the  $d = 0.4$  representation depends on whether the retained persistence is economically meaningful - a question addressed empirically in the forecasting experiments of Sections 5 and 6.

## 5. MLP Forecasting with Joint Lag and Hyperparameter Tuning

### 5.1 Problem Formulation and Supervised Learning Setup

We frame one-step-ahead forecasting as a supervised regression problem by converting the univariate series  $\{y_t\}_{t=1}^T$  into a design matrix via lag embedding. For a candidate lag length  $L \in \mathcal{L}$ , the feature vector is

$$X_t = [y_{t-1}, y_{t-2}, \dots, y_{t-L}]^\top \in \mathbb{R}^L, \quad \text{with response } y_t, \quad (7)$$

for all  $t$  such that the  $L$  required lags exist, yielding a design matrix  $X \in \mathbb{R}^{N \times L}$  and response vector  $y \in \mathbb{R}^N$  with  $N = T - L$ . The forecast target is strictly one-step-ahead and uses only lagged realizations, with no contemporaneous or future information incorporated into the feature set - a requirement that is essential for causal validity in time-series forecasting (Box et al.).

To preserve the chronological ordering of the data and avoid look-ahead bias, we employ a strict temporal train-test split with test fraction  $\alpha = 0.20$ . The first  $(1 - \alpha)N$  observations form the training set and the remaining  $\alpha N$  form the test set. Feature standardization uses a scaler fitted exclusively on the training data, with training-derived mean and standard deviation applied to the test set:

$$\tilde{X}_{\text{train}} = \text{Std}(X_{\text{train}}), \quad \tilde{X}_{\text{test}} = \text{Std}_{\text{train}}(X_{\text{test}}), \quad (8)$$

so that the test set exerts no influence on the scaling parameters. As a benchmark, we employ the naive last-value forecast  $\hat{y}_t^{\text{naive}} = y_{t-1}$ , which is known to be difficult to beat for persistent processes (Meese and Rogoff) and serves as a strong practical reference.

### 5.2 MLP Architecture and Hyperparameter Search

The MLP maps  $\mathbb{R}^L \rightarrow \mathbb{R}$  through a stack of fully-connected layers:

$$f_\theta(X_t) = W_K \phi(\dots \phi(W_2 \phi(W_1 X_t + b_1) + b_2) \dots) + b_K, \quad (9)$$

where  $\phi(\cdot)$  is a ReLU nonlinearity (Nair and Hinton). The universal approximation theorem (Hornik et al.) guarantees that sufficiently deep or wide MLPs can represent any continuous function to arbitrary accuracy, providing theoretical justification for the architecture. Hyperparameters - number of hidden layers ( $K \in \{1, \dots, 6\}$ ), units per hidden layer ( $\{16, 32, \dots, 256\}$ ), dropout rate

(Srivastava et al.) ( $\{0.0, 0.1, 0.2, 0.3\}$ ), batch normalization (Ioffe and Szegedy) (on/off), and Adam (Kingma and Ba) learning rate (log-uniform on  $[10^{-4}, 5 \times 10^{-3}]$ ) are selected using the Keras Tuner Hyperband algorithm. All models minimize mean absolute error (MAE) on the training set with an internal 20% validation split; early stopping restores the best weights and reduces overfitting.

Lag length  $L$  changes the input dimensionality and must be tuned in an explicit outer loop over a candidate grid  $\mathcal{L}$ . For each candidate  $L$ , we construct the lagged dataset, apply the chronological split, run a Hyperband search to identify the best MLP configuration, and record the best validation loss. The lag length  $L^*$  achieving the minimum validation loss is selected for the final model. After identifying  $L^*$  and the associated architecture, batch size is further refined over  $\{16, 32, 64, 128\}$  by selecting the value yielding the lowest validation loss under early stopping. Out-of-sample performance is shown for both the tuned MLP and the naive benchmark using MAE, RMSE,  $R^2$ , and the Pearson correlation between predictions and realized values.

### 5.3 Empirical Results

The forecasting framework was applied independently to the three representations of the same underlying process: raw levels, log returns, and the fractionally differenced series ( $d = 0.4$ ). Figures 5 and 6 shows the forecast trajectories overlaid on the realized test-set observations for each series.

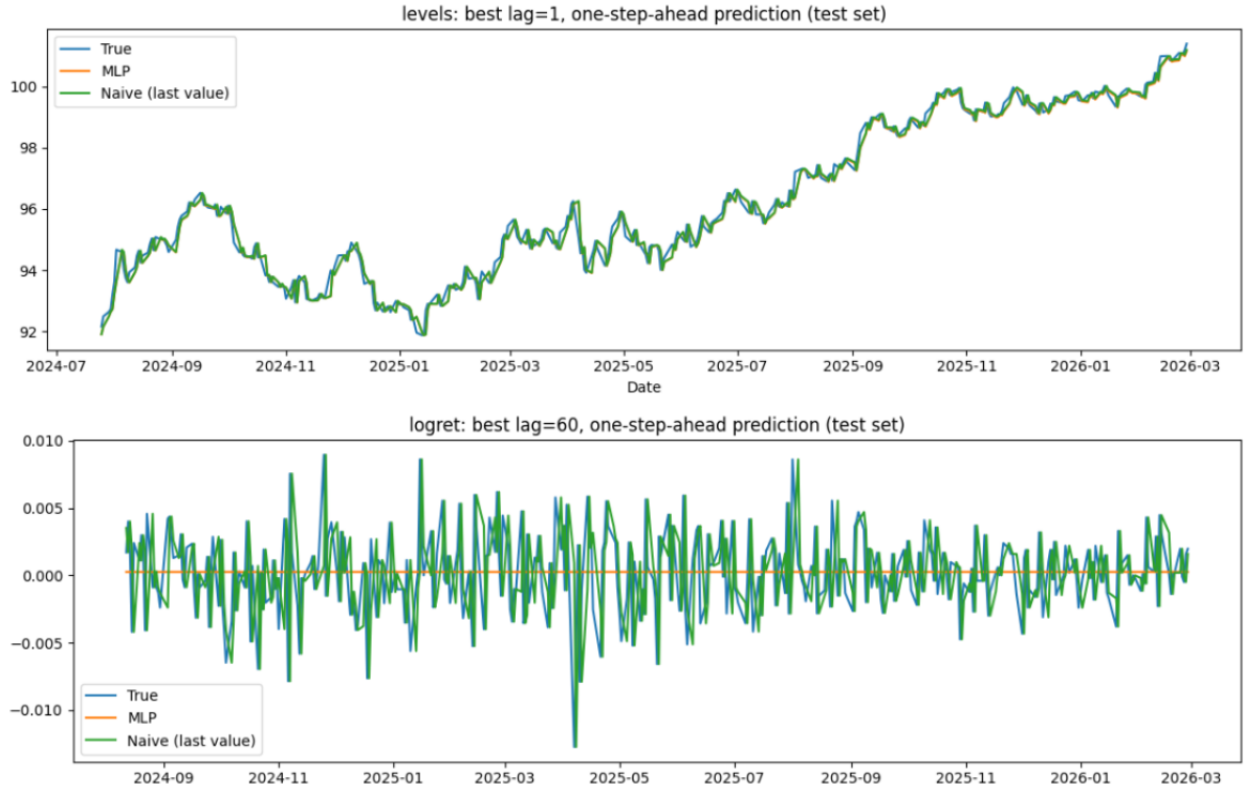
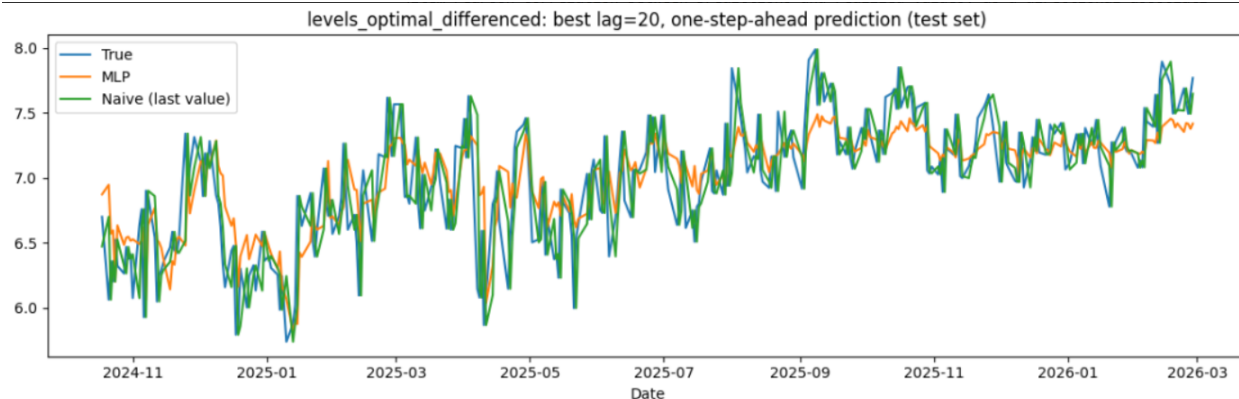


Figure 5: MLP and naive benchmark forecast trajectories for levels and log returns on the test segment.



```

=== Comparison (lower MAE/RMSE better; higher R2 better) ===
Series BestLag MLP_MAE MLP_RMSE MLP_R2 Naive_MAE Naive_RMSE Naive_R2 LR Layers BatchNorm Dropout BatchSize
logret 60 0.002180 0.002818 -0.000383 0.003100 0.003949 -0.964560 0.002584 4 False 0.3 128
levels 1 0.215841 0.278202 0.987205 0.213298 0.275655 0.987438 0.004389 3 False 0.0 128
levels_optimal_differenced 20 0.230536 0.298912 0.570475 0.229011 0.295495 0.580239 0.002966 5 False 0.2 16

```

Figure 6: MLP and naive benchmark forecast trajectories for the fractionally differenced series ( $d = 0.4$ ) on the test segment.

**Raw levels..** The tuning procedure selected a lag length of  $L = 1$ , consistent with the near unit-root dynamics documented in Section 2. With only the immediately preceding observation as input, the MLP learns a near-identity mapping, and its forecast closely overlaps with the naive benchmark throughout the test period. Both achieve near-identical error magnitudes (MAE  $\approx 0.216$  for the MLP versus  $\approx 0.213$  for the naive forecast) and  $R^2 \approx 0.987$ , indicating that almost all predictable variation arises from simple persistence rather than nonlinear structure. This outcome is theoretically expected: when the underlying process is nearly random walk, the conditional expectation  $\mathbb{E}[y_t | y_{t-1}]$  is well approximated by the identity  $y_{t-1}$ , leaving little room for additional modeling capacity (Campbell and Shiller).

**Log returns..** The return series exhibits substantially weaker serial dependence, and the tuning procedure selected a longer memory window ( $L = 60$ ), reflecting the possibility of weak predictive signals at longer horizons. Despite this, the resulting MLP forecast is essentially flat around zero throughout the test sample, while realized returns fluctuate with high volatility. The MLP achieves MAE  $\approx 0.00218$  - marginally better than the naive benchmark (MAE  $\approx 0.00310$ ) - and an  $R^2$  of approximately  $-0.00038$ , indicating performance no better than the unconditional mean predictor. These results are in line with the efficient market hypothesis under weak-form informational efficiency (Fama): past return information contains minimal predictive content for next-day returns, and the neural network effectively learns that the optimal forecast is close to zero.

**Fractionally differenced levels..** The optimally differenced series presents an intermediate case. The lag-selection procedure identified  $L = 20$ , and the MLP achieves MAE  $\approx 0.231$  and RMSE  $\approx 0.299$ , with  $R^2 \approx 0.57$ , indicating that a good portion of the predictable variation in the transformed

process is captured. Unlike the level series, where the MLP and naive benchmark are essentially identical, the MLP outperforms the naive forecast in certain local segments of the test set and provides smoother tracking of the series’ broader dynamics. This result is consistent with the design objective of the fractional differencing transformation: retaining moderate temporal dependence that nonlinear models can exploit, while removing the dominant stochastic trend that renders the naive forecast nearly optimal for raw levels.

**Cross-series synthesis.** The empirical pattern across the three transformations reveals a structural principle: the effectiveness of machine learning models depends not on architectural expressiveness alone, but critically on the signal-to-noise properties of the input representation (Gu et al.). Raw levels are dominated by persistence, for which the naive last-value forecast is nearly Bayes-optimal; log returns exhibit minimal predictable linear structure, causing the network to converge toward a near-zero forecast; the fractionally differenced representation offers the most favorable trade-off, where moderate dependence survives but extreme persistence has been attenuated. These findings reinforce the view that appropriate preprocessing and stationarity-inducing transformations play a central role in extracting predictive signals from financial time series (López de Prado).

## 6. CNN Forecasting via Gramian Angular Field Representations

### 6.1 Converting Time Series to Images via Gramian Angular Fields

Convolutional neural networks (LeCun et al., “Backpropagation”) require structured two-dimensional inputs and are not directly applicable to raw numerical time-series vectors. To bridge this gap, we employ the Gramian Angular Field (GAF) methodology of Wang and Oates, which encodes a univariate time-series window into a two-dimensional image that preserves temporal dependencies and structural patterns accessible to convolutional feature detectors. The GAF construction occurs in three steps. First, the time series within a rolling window of length  $W$  is rescaled to the interval  $[-1, 1]$  via min-max normalization. Second, each rescaled observation  $\tilde{y}_{t-k} \in [-1, 1]$  is mapped to an angular value in polar coordinates via

$$\phi_{t-k} = \arccos(\tilde{y}_{t-k}), \quad k = 0, 1, \dots, W - 1. \tag{10}$$

Third, a Gram matrix is constructed using the cosine of the pairwise sum of angles:

$$G_t(i, j) = \cos(\phi_{t-i} + \phi_{t-j}), \quad i, j \in \{0, 1, \dots, W - 1\}, \tag{11}$$

giving a symmetric  $W \times W$  image that encodes pairwise temporal relationships across the window. The diagonal entries recover the original rescaled series, while off-diagonal entries encode inter-temporal correlations. The GAF representation has been shown to be effective for time-series classification tasks where recurring patterns, motifs, or regime signatures are discriminative features

(Wang and Oates; Fawaz et al.).

Figures below show the GAF encoding process and resulting image representations for the level, log-return, and fractionally differenced series.

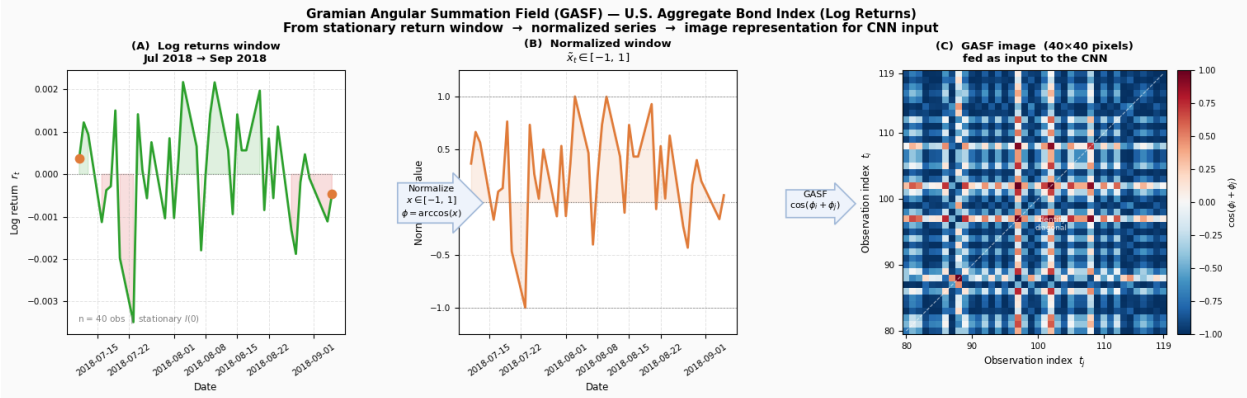


Figure 7: GAF encoding pipeline and the corresponding image representation for the level series.

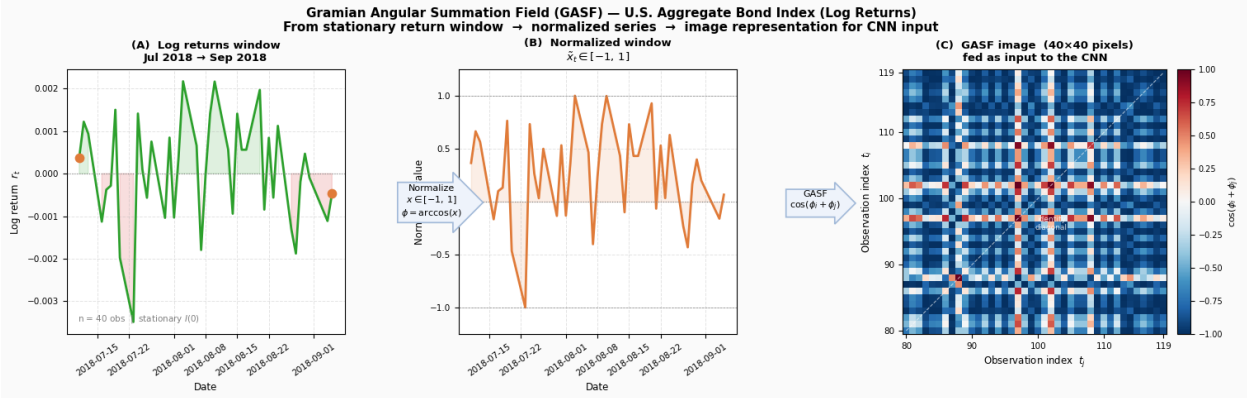


Figure 8: GAF encoding pipeline and the corresponding image representation for the log-return series.

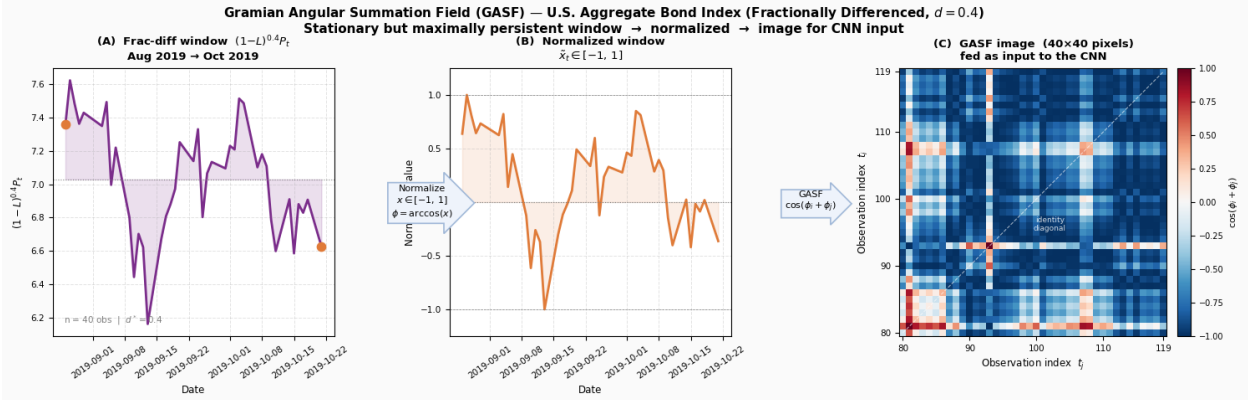


Figure 9: GAF encoding pipeline and the corresponding image representation for the fractionally differenced series ( $d = 0.4$ ).

## 6.2 CNN Architecture and Training

For each input representation, a CNN is trained for one-step-ahead regression using GAF images as inputs. The architecture consists of stacked convolutional layers with ReLU activations (Nair and Hinton) and max-pooling, followed by fully connected layers mapping to a scalar output. Training uses the same chronological 80–20 train/test split as the MLP experiments, with out-of-sample evaluation on the held-out 20% test segment. A window length of  $W = 20$  observations is used across all series for comparability.

## 6.3 Out-of-Sample Results and Interpretation

Table 10 reports out-of-sample prediction performance for the CNN–GAF models over the three input representations.

Table 10: CNN–GAF out-of-sample prediction performance across three input representations (test set, 20% holdout, horizon  $h = 1$ ).

Input Series	RMSE	MAE	$R^2$
Levels (non-stationary, $I(1)$ )	5.823	4.829	−4.683
Log Returns (stationary, $I(0)$ )	0.004	0.003	−0.806
Frac. Diff. ( $d = 0.4$ , near-stationary)	0.871	0.750	−2.646

A consistent pattern emerges across all three representations: every CNN–GAF model gives a negative out-of-sample  $R^2$ , indicating performance inferior to a naive mean predictor at every step. The levels model produces the largest absolute errors (RMSE = 5.82, MAE = 4.83) and the most negative  $R^2$  ( $= -4.68$ ), a direct consequence of feeding a non-stationary series into a model trained on a different distributional regime than the one it encounters at test time. Because GAF images are constructed from min-max-normalized windows, the global rescaling is determined by

local window extrema, which can shift systematically as the level series trends through time; the CNN thus faces a distribution shift between training and test images that is more severe than what the MLP encounters with standardized lag vectors.

The log-return model achieves the smallest raw errors (RMSE = 0.004, MAE = 0.003), reflecting the narrow range of return fluctuations. However, an  $R^2$  of  $-0.81$  reveals that the model cannot beat the mean predictor, indicating that the CNN model fails to extract any net predictive signal from the GAF representation of return series. A plausible mechanism is that high-frequency noise and heteroskedasticity, which dominate the return series, translate into distinctive but unpredictable visual artifacts in the GAF images; the CNN may fit these artifacts in-sample while generalizing poorly out-of-sample.

The fractionally differenced model ( $d = 0.4$ ; RMSE = 0.871,  $R^2 = -2.65$ ) occupies an intermediate position in raw error magnitude, but its  $R^2$  is more negative than the log-return model. A likely explanation is that the  $W = 20$  window used to construct each GAF image truncates the very long-memory information that fractional differencing was designed to preserve; the CNN model is effectively asked to learn long-memory dynamics from a short-memory image, creating an information bottleneck. Additionally, with a limited number of training epochs and a relatively modest architecture, the CNN may fail to identify the subtle linear mappings from image features to the next-step target, or may overfit transient image artifacts that do not generalize. Figure 10 summarizes the predictive performance diagnostics for all three CNN–GAF models.

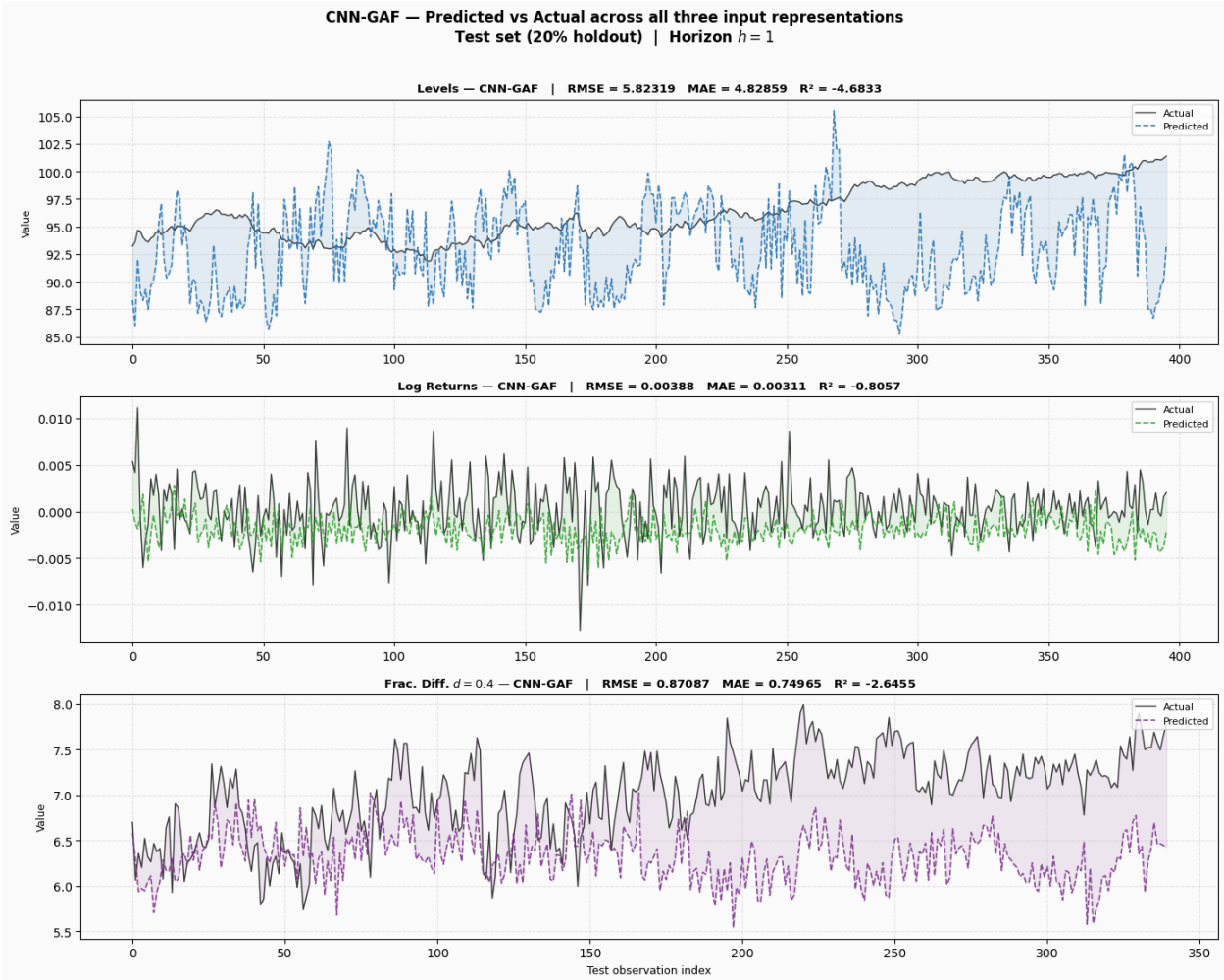


Figure 10: Evaluation of predictive performance for CNN-GAF models across the three input representations.

## 7. Comparative Discussion: MLP versus CNN-GAF

### 7.1 Inductive Bias and Representation

The sharp empirical divergence between MLP and CNN-GAF performance is best understood through the lens of inductive bias (LeCun et al., “Deep Learning”) - the set of assumptions each architecture embeds about the structure of the learning problem. The MLP receives the last  $L$  values as an ordered numerical vector and learns a nonlinear mapping  $\hat{y}_t = f_\theta(y_{t-1}, \dots, y_{t-L})$  in which temporal ordering is persisted explicitly by the feature construction. For level-like series, the MLP can easily represent persistence-dominated dynamics by learning a near-identity map on the first lag, directly approximating the Bayes-optimal forecast under near-random-walk dynamics. The CNN model, in contrast, operates on a GAF image  $G_t \in \mathbb{R}^{W \times W}$  that emphasizes pairwise angular relationships among points in a window, rather than the original numerical scale of the series. This

representation is powerful when the forecasting problem depends on shape, motifs, or recurring local patterns (Wang and Oates; Fawaz et al.) - but it is not naturally aligned with persistence-driven dynamics, where the most informative single statistic for next-step prediction is the immediately preceding value  $y_{t-1}$ .

For the  $I(1)$  level series, the Bayes-optimal one-step predictor is close to the identity  $\hat{y}_t \approx y_{t-1}$ , and the MLP achieves this by selecting  $L = 1$  and learning the corresponding function. The CNN-GAF pipeline introduces an intermediate representation that is not tailored to identity-like forecasting: the GAF matrix may primarily encode the smoothness or curvature of the local trajectory, discarding the simplest sufficient statistic for the one-step prediction problem. For the return series, weak predictability under the efficient market hypothesis (Fama) causes both architectures to collapse toward trivial forecasts, but the MLP is less prone to fitting spurious visual artifacts induced by the GAF transform, because MAE-minimizing training with early stopping tends to shrink toward a conservative near-zero predictor. For the fractionally differenced series, the residual persistence is naturally expressed in lag space, and the MLP can approximate the implied smooth nonlinear corrections; the CNN-GAF pipeline likely suffers from the combination of a short window (information bottleneck) and sensitivity to transient image-level artifacts.

## 7.2 Practical Implications

The results support a pragmatic conclusion: for one-step-ahead forecasting of highly persistent financial levels and weakly autocorrelated returns, direct lag-based models - including linear baselines and modest nonlinear MLPs - are competitive and often difficult to improve upon. CNNs operating on GAF images may be more appropriate when the forecasting problem is genuinely pattern-based - for example, classification of market regimes, detection of recurring structural motifs, or multi-step horizon prediction where the shape of recent dynamics provides discriminative information (Fawaz et al.; Ismail Fawaz et al.). In the present application, the non-stationarity of levels, the near-randomness of returns under weak-form efficiency (Fama), and the long-memory nature of the fractionally differenced series collectively favor architectures that preserve the temporal ordering and numerical scale of lags. This reinforces the central message of this paper: the choice of series transformation and the alignment between architectural inductive bias and the statistical properties of the data are often more consequential for predictive performance than architectural complexity per se (Gu et al.; López de Prado).

## 8. Conclusion

This paper investigated the statistical properties and short-horizon predictability of the U.S. Aggregate Bond Index using modern deep learning methods, with emphasis on series transformation and architectural inductive bias. Index levels are found to be  $I(1)$  processes with near-unit-root persistence and slowly decaying autocorrelations, while log returns are  $I(0)$  with weak serial dependence, volatility clustering, and fat tails. Applying the fractional differencing procedure of López de Prado yields an optimal order of approximately  $d^* \approx 0.40$ – $0.45$ , producing a near-stationary representation that preserves low-frequency memory relative to full first differencing (Granger and Joyeux; Hosking).

Forecasting experiments show that MLP models trained on lagged vectors achieve near-baseline performance for levels (driven by persistence), near-zero performance for returns (consistent with weak-form efficiency (Fama)), and the strongest incremental performance for the fractionally differenced series, where moderate dependence remains. CNN–GAF models produce uniformly negative out-of-sample  $R^2$  across all representations, suggesting a mismatch between the geometric image encoding and the persistence-dominated one-step forecasting task.

Overall, predictive performance is driven primarily by the transformation of the underlying series—its stationarity and memory structure—rather than model complexity. For practitioners in fixed-income machine learning, this highlights the importance of preprocessing and aligning model inductive bias with the statistical structure of the data before deploying sophisticated architectures. Future work may examine whether richer feature sets (cross-asset signals, macroeconomic indicators, or term-structure variables), alternative architectures such as LSTMs (Hochreiter and Schmidhuber) or attention-based transformers, or longer forecast horizons alter these conclusions, and whether CNN–GAF methods are better suited for classification or regime-detection tasks.

## A. Appendix: Fractional Differencing - Weights and Implementation

The fractional differencing operator  $(1 - L)^d$  produces weights

$$w_k = (-1)^k \binom{d}{k} = (-1)^k \frac{d(d-1)\cdots(d-k+1)}{k!}, \quad (12)$$

with  $w_0 = 1$ ,  $w_1 = -d$ ,  $w_2 = d(d-1)/2$ , etc. For large  $k$ , the weights decay at the hyperbolic rate  $|w_k| \sim k^{-(1+d)}$ , in contrast to the finite-memory operator obtained at  $d = 1$ , where all weights beyond  $k = 1$  are exactly zero. This slow, hyperbolic decay is the defining property of long-memory processes and distinguishes fractional differencing from exponential decay models (Hosking; Granger and Joyeux). In practice, the infinite sum is truncated at a finite lag  $K$  determined by a weight-threshold criterion ( $|w_K| < \epsilon$ , typically  $\epsilon = 10^{-5}$ ), a fixed window, or a cumulative weight criterion. Truncation introduces a trade-off: larger  $K$  preserves more long-memory structure but reduces the effective sample size to  $T_{\text{effective}} = T - K$  and increases computational cost; smaller  $K$  improves efficiency but approximates the infinite operator more coarsely. When  $d = 1$ , the operator collapses to the standard first-difference operator  $(1 - L)$ , recovering  $\tilde{P}_t = P_t - P_{t-1}$  with finite memory (Box et al.). For  $d \in (0, 1)$ , the operator applies a low-pass filter that attenuates stochastic trend components while preserving long-memory dependence - the “stationary but maximally persistent” transformation advocated by López de Prado.

## References

- Baillie, Richard T. “Long Memory Processes and Fractional Integration in Econometrics.” *Journal of Econometrics*, vol. 73, no. 1, 1996, pp. 5–59.
- Bollerslev, Tim. “Generalized Autoregressive Conditional Heteroskedasticity.” *Journal of Econometrics*, vol. 31, no. 3, 1986, pp. 307–327.
- Box, George E. P., et al. *Time Series Analysis: Forecasting and Control*. 5th ed., Wiley, 2015.
- Campbell, John Y., and Robert J. Shiller. *The Econometrics of Financial Markets*. Princeton University Press, 2012.
- Cont, Rama. “Empirical Properties of Asset Returns: Stylized Facts and Statistical Issues.” *Quantitative Finance*, vol. 1, no. 2, 2001, pp. 223–236.
- Dickey, David A., and Wayne A. Fuller. “Distribution of the Estimators for Autoregressive Time Series with a Unit Root.” *Journal of the American Statistical Association*, vol. 74, no. 366, 1979, pp. 427–431.
- Engle, Robert F. “Autoregressive Conditional Heteroscedasticity with Estimates of the Variance of United Kingdom Inflation.” *Econometrica*, vol. 50, no. 4, 1982, pp. 987–1007.
- Engle, Robert F., and Clive W. J. Granger. “Co-Integration and Error Correction: Representation, Estimation, and Testing.” *Econometrica*, vol. 55, no. 2, 1987, pp. 251–276.
- Fama, Eugene F. “Efficient Capital Markets: A Review of Theory and Empirical Work.” *Journal of Finance*, vol. 25, no. 2, 1970, pp. 383–417.
- Fawaz, Hassan Ismail, et al. “Deep Learning for Time Series Classification: A Review.” *Data Mining and Knowledge Discovery*, vol. 33, no. 4, 2019, pp. 917–963.
- Granger, Clive W. J., and Roselyne Joyeux. “An Introduction to Long-Memory Time Series Models and Fractional Differencing.” *Journal of Time Series Analysis*, vol. 1, no. 1, 1980, pp. 15–29.
- Gu, Shihao, et al. “Empirical Asset Pricing via Machine Learning.” *Review of Financial Studies*, vol. 33, no. 5, 2020, pp. 2223–2273.
- Hamilton, James D. *Time Series Analysis*. Princeton University Press, 1994.
- Hochreiter, Sepp, and Jürgen Schmidhuber. “Long Short-Term Memory.” *Neural Computation*, vol. 9, no. 8, 1997, pp. 1735–1780.
- Hornik, Kurt, et al. “Multilayer Feedforward Networks Are Universal Approximators.” *Neural Networks*, vol. 2, no. 5, 1989, pp. 359–366.
- Hosking, J. R. M. “Fractional Differencing.” *Biometrika*, vol. 68, no. 1, 1981, pp. 165–176.
- Ioffe, Sergey, and Christian Szegedy. “Batch Normalization: Accelerating Deep Network Training by Reducing Internal Covariate Shift.” *Proceedings of the 32nd International Conference on Machine Learning*, 2015, pp. 448–456.

- Ismail Fawaz, Hassan, et al. “InceptionTime: Finding AlexNet for Time Series Classification.” *Data Mining and Knowledge Discovery*, vol. 34, no. 6, 2019, pp. 1936–1962.
- Kingma, Diederik P., and Jimmy Ba. “Adam: A Method for Stochastic Optimization.” *arXiv*, 2014, arXiv:1412.6980.
- LeCun, Yann, et al. “Backpropagation Applied to Handwritten Zip Code Recognition.” *Neural Computation*, vol. 1, no. 4, 1989, pp. 541–551.
- . “Deep Learning.” *Nature*, vol. 521, no. 7553, 2015, pp. 436–444.
- López de Prado, Marcos. *Advances in Financial Machine Learning*. Wiley, 2018.
- Mandelbrot, Benoit B. “The Variation of Certain Speculative Prices.” *Journal of Business*, vol. 36, no. 4, 1963, pp. 394–419.
- Meese, Richard A., and Kenneth Rogoff. “Empirical Exchange Rate Models of the Seventies: Do They Fit Out of Sample?” *Journal of International Economics*, vol. 14, no. 1–2, 1983, pp. 3–24.
- Nair, Vinod, and Geoffrey E. Hinton. “Rectified Linear Units Improve Restricted Boltzmann Machines.” *Proceedings of the 27th International Conference on Machine Learning*, 2010, pp. 807–814.
- Nelson, Charles R., and Charles R. Plosser. “Trends and Random Walks in Macroeconomic Time Series: Some Evidence and Implications.” *Journal of Monetary Economics*, vol. 10, no. 2, 1982, pp. 139–162.
- Rumelhart, David E., et al. “Learning Representations by Back-Propagating Errors.” *Nature*, vol. 323, no. 6088, 1986, pp. 533–536.
- Said, Said E., and David A. Dickey. “Testing for Unit Roots in Autoregressive-Moving Average Models of Unknown Order.” *Biometrika*, vol. 71, no. 3, 1984, pp. 599–607.
- Srivastava, Nitish, et al. “Dropout: A Simple Way to Prevent Neural Networks from Overfitting.” *Journal of Machine Learning Research*, vol. 15, no. 1, 2014, pp. 1929–1958.
- Wang, Zhiguang, and Tim Oates. “Imaging Time-Series to Improve Classification and Imputation.” *Proceedings of the 24th International Joint Conference on Artificial Intelligence*, 2015, pp. 3939–3945.